

誌 謝

這本拙作及這個實驗的誕生，是由很多人的共同參與，很多可能是最好，甚至是唯一的人與物所做的貢獻；而我，只是將之做最完美的結合，呈現出來的推手而已。首先要感謝的是我的指導教授朝春光老師這兩年來的諄諄教悔與細心照顧，在我還幻想著 nanoarray“應該”沒問題時，老師“務實”的精神喊話，讓我從“再應該下去應該會畢不了業”，到不再做白日夢的務實態度；以及在相互討論的腦力激蕩下，半夜突發其想寄 e-mail 給老師，老師馬上回我“祺淵，你該早點睡了”；老師的指導讓我發覺自己的許多盲點與缺失，讓即將離開的我得以不同以往。接著感謝所上謝宗雍老師對實驗的指教，與很多正確觀念的嚴謹要求，及對論文修改的不遺餘力，使我了解到自己更多的欠缺與不足，讓我銘感腑內，永銘於心。再來，是本實驗的最大股東，有“唬神”、“大鬍子”之稱，永遠看見我沒瞧到的地方，點破我想不透的思維，在我心思困頓時鼓勵我奮力向前，要我持續急徐前行，讓人永遠敬重，記得照顧別人卻忘了照料自己的大師兄仁君學長，這段日子以來若無大師兄的鼓勵與提攜，今天的我絕對無法得以成長，若無學長的幫忙，這實驗不可能得以實現。接下來，感謝一起修課，一起哈拉聊天的養國學長，日常點滴與知識上的分享，讓我的思緒時常保持開朗的狀態，讓我的態度永遠樂觀向前。再來，感謝欣瑩學姊在實驗檢測上的幫忙，讓我不會手足無措，在生活鎖事上的分享，讓我免於持有負面的情緒。感謝國強學長在材料電性、文獻查詢與簡報技術上的教導，讓我學到很多自己以前不懂，不曾碰觸過的領域，也讓我很多技能得以提昇。感謝兆鼎學長在修課上的分享，及實驗程序上的幫忙，讓我不至於已經兩個頭大的頭再繼續大下去。感謝定侃學長在 TEM 上的幫忙，解決了我燃眉之急。感謝俊沐學長在實驗上意見的分享，讓我得以用不同的思路考量我的作法。感謝建仲學長在熱力學、電化學和文獻回顧上的指導，與很多知識上的分享，讓我的不知得以了解，知識得以延伸。感謝金國學長、同窗同學政翰、學弟建財、學妹蓉萱在實驗及生活上的幫忙；特別是長得很像我表妹的學妹家茵，在儀器預約及日常鎖事上的幫忙，讓我得以按步就般地將實驗如期進行。緊接著，感謝鐵鋁錳三劍客何春伯、彭英銘、林志龍在修課、實驗及生活點滴上的分享與幫忙，尤其是在交大最有緣的同學Y龍，一起為考研究所而打拼，又一起來到交大為實驗而賣命，捨自己儀器操作時段的鼎力相助上，讓我得以在破記錄被停權的同時，仍可破記錄的繼續給它作下去。感謝鐵鋁錳三劍客第二代學弟Y堯、陞哥、小傑在修課與實驗儀器上的幫忙，使我不會持續抱著頭燒。感謝電物所李明知老師實驗室古慶順學長在半導體發光知識上的細心教導及儀器檢測上的幫忙，讓我所了解的知識得以連結，對半導體發光能有更進一步的認識。感謝機械所二技同學明瑜、建溢在日常生活上的幫忙與分享，讓緊湊的研究生活得以更多采多滋。感謝台科曾東陽老師幫我安排每個月 FE-SEM 的時段，讓我得以照出相當多關鍵且非常漂亮到不行的照片。感謝中山材料所陳惠香小姐在 CL 檢測

上的幫忙與經驗上的分享，使我獲益良多。感謝北科材料大師李正中老師在材料知識上的賣命傳授與細心教導，讓我這個旁門外漢得以有考取材料所的機會。感謝台科班導王朝正老師，以及雷添壽老師在知識領域的傳授及態度觀點上的提攜與要求，讓我得以能全面性的思考自己所面臨到的問題，及探索其解決之道。感謝專科同學大全、俊賢、貴雄、春賢，二技同學嘉恩、小胡、Y志、小呈、Y福、TACO、衍慶、同梯坤敏及一堆隨時 call 來東南西北瞎扯，543 瞎聊，生活點滴分享的同學朋友，讓我在面對乏味的實驗時，得以更加體認到自己並不是一個人在做。

接下來，要感謝我生命中最重要的三號人物：將來絕對是個奇才的老弟祺豐，在我離家求學時扛起陪伴父母的重責大任，和我分享生活點滴，大話家常，聽我亂扯一堆有的沒有的。以及我最親愛的老爸、老媽，隨時告誡我許多人生大道理；在我吃飯時打電話來要我不要忘記洗澡，洗澡時打來要我記得早點睡覺，睡覺時打來問我吃飯了沒。從小到大父母的辛勤付出，永遠點滴在心頭，那是我永遠的 *driving force*。

最後，感謝老天爺恩賜我機會，讓今日的我得以拙壯成長，希望明日的我能貢獻自己所學一切。



汽相蒸鍍四支柱單晶氧化鋅其自組性質及光電特性之研究

學生：林祺淵

指導教授：朝春光 博士

國立交通大學材料科學與工程研究所

摘 要

本研究以不同於水平爐管之方式，採用近似密閉系統之垂直式汽相蒸鍍法來合成四支柱氧化鋅。多量有方向性的四支柱單晶氧化鋅如預期般地不藉由觸媒物產出於基材上。有方向性的四支柱氧化鋅藉由汽相-固化過程產出於矽基板及三氧化二鋁薄膜模板上。再者，藉由調控空氣、水蒸汽、過氧化氫之實驗參數來生成具高長徑比及多樣型貌的四支柱氧化鋅。消波塊狀的四支柱氧化鋅圓徑 100 奈米到超過 1 微米，長度超過 10 微米大量生成於基材上。於富氧濃度的反應裡，四支柱晶體更會朝其 basal plane 方向成長，且成長模式顯現出層層堆疊的螺旋方式。其晶體裡的含氧變化不僅影響其成長方位，也改變了其激發光效應。

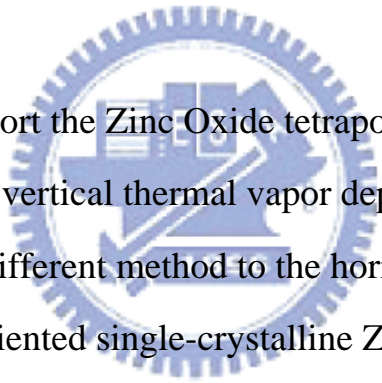
On Self-Assembly and Optoelectronic Properties for the Single-Crystalline ZnO Tetrapods by Vapor Deposition

student : Chi-Yuan Lin

Advisors : Dr. Chuen-Guang Chao

Institute of Materials Science and Engineering
National Chiao Tung University

ABSTRACT



In this letter, we report the Zinc Oxide tetrapods synthesized in quasi-closed system by vertical thermal vapor deposition in box furnace, which demonstrates a different method to the horizontal tube. As expected, fairly well-oriented single-crystalline ZnO tetrapods grew on the substrates without catalyst. The oriented growth of ZnO tetrapods had uniform shape and length, and had been accomplished on the silicon wafer and alumina-membrane template (AAM) *via* a vapor-solid (VS) process. Otherwise, by harnessing the experimental conditions—air, H₂O vapor, and H₂O₂ vapor atmospheres—ZnO tetrapods had synthesized with various morphologies and high aspect ratios. Such ZnO tetrapods, typically 100 nm to over 1 μ m in diameter and up to about 10 μ m in length, were oriented in armor-unit-shape fashion and aggregated in the large yield on the substrates. The crystal growth of rods for tetrapods appeared to be helical like growth by layer-by-layer, and crystals

preferred to grow toward the basal plane in rich oxygen concentration for reaction atmosphere. Oxygen contain for ZnO tetrapods influenced not only the orientation of growth but also the luminescence properties of its.



Contents

Abstract (in Chinese)	I
Abstract (in English)	II
Contents	IV
List of Figures	VI
Chapter 1 Introduction	1
1.1 A brief review.....	1
1.2 Motivation.....	1
1.3 Organization of the thesis.....	2
Chapter 2 Literatural Review	3
2.1 A Briefly introduction of ZnO	3
2.2 Fabrication Methods of Oriented ZnO.....	4
2.3 Luminescent Properties of Oriented ZnO.....	5
2.4 Crystal Structure and Growth Mechanism of Oriented ZnO	6
Chapter 3 Experimental Process	20
3.1 Experimental Apparatus.....	20
3.2 Sample Preparation	21
3.3 Characterization of the Morphologies and Structures.....	22
Chapter 4 Results and Discussions	24

4.1	The Effects of Growth Ambience of ZnO Tetrapods.....	24
4.1.1	The air atmosphere.....	24
4.1.2	The H ₂ O atmosphere.....	25
4.1.3	The H ₂ O ₂ atmosphere.....	25
4.2	The CL spectra of ZnO Tetrapods.....	27
4.3	Crystal Growth and Mechanisms of Oriented ZnO Structures..	28
Chapter 5	Conclusions.....	47
Reference.....		48



List of Figures

Chapter 2

- Fig. 2.1 Schematic illustration of the chemical vapor transport and condensation experimental set-up for ZnO nanowire growth ^[1]9
- Fig. 2.2 (A through E) SEM images of ZnO nanowire arrays grown on sapphire substrates. A top view of the well-faceted hexagonal nanowire tips is shown in (E). (F) High-resolution TEM image of an individual ZnO nanowire showing its $\langle 0001 \rangle$ growth direction ^[7]9
- Fig. 2.3 SEM images of ZnO tetrapods with different diameters. a) ZnO tetrapods with arms of 200 nm diameter. b) ZnO tetrapods with arms of 2 μ m diameter. c) High-magnification SEM image of a single ZnO tetrapod with an arm of 2 μ m diameter ^[11]10
- Fig. 2.4 a) TEM image of a tripod. b) Dark field image of arm I recorded on the $[10\bar{2}]$ spot along the $[201]$ zone axis. The inset is the SAD pattern of arm I of the tripod. c) High-resolution TEM image at the joint of the tripod ^[11]10
- Fig. 2.5 SEM images of ZnO tetrapods with trumpet-like arms at low (a) and (b) magnification ^[11]10
- Fig. 2.6 SEM images of self-assembled ZnO tetrapods. a) A Low-magnification SEM image of ZnO tetrapods with trumpet-shaped arms. The inset image is a tetramer formed from the ZnO tetrapods. b) Staggered from of the ZnO tetrapod dimmer. c) Eclipsed from of the ZnO tetrapod dimmer ^[11]11
- Fig. 2.7 SEM images of ZnO nanostructures: a) tetrapods (left) and rods (right) obtained in air; b) small tetrapods (left) and mixture of tetrapods and wires (right) obtained in dry argon flow; and c) mixture of tetrapods and wires obtained in humid argon flow ^[32]11
- Fig. 2.8 Representative SEM images of a) undoped ZnO, b) Mn diffusion doped ZnO ^[46]12
- Fig. 2.9 Representative SEM images of ZnO nanostructures: a) ZnO prepared from Zn. b) ZnO prepared from ZnO:C. c) ZnO prepared from ZnO:C:GeO₂ ^[47]12

Fig. 2.10 Photoluminescence of ZnO nanostructures prepared under different conditions ^[32]	13
Fig. 2.11 Photoluminescence of undoped and Mn doped ZnO tetrapod structures ^[46]	13
Fig. 2.12 PL spectrum measured at room temperature from ZnO structures prepared from different materials ^[47]	14
Fig. 2.13 SEM images showing the three typical morphologies of the as-prepared ZnO products. a) needle-like rods. b) nanoribbons. c) nanowires ^[26]	15
Fig. 2.14 PL spectra recorded at room temperature. Spectra a, b, and c were recorded from the low temperature site nanowires, the medium temperature site nanoribbons, and the high temperature site needle-like rods, respectively ^[26]	15
Fig. 2.15 FE-SEM images of ZnO nanowire arrays on m-sapphire. a) and b) perspective view (45°) of the nanowires with growth duration 30 and 10 min, respectively. Scale bar: 1μm. c) and d) corresponding top views. Scale bar: 500nm ^[48]	16
Fig. 2.16 Photoluminescence spectra of ZnO nanowires at room temperature using 325 nm line of a He-Cd laser as the excitation source ^[48]	16
Fig. 2.17 The wurtzite structure model of ZnO. The tetrahedral coordination of Zn-O is shown ^[50]	17
Fig. 2.18 Typical growth morphologies of one-dimensional ZnO nanostructures and the corresponding facets ^[50]	17
Fig. 2.19 a) Low-magnification SEM image of the as-synthesized ZnO nanorings. b) High-magnification SEM image of a freestanding single-crystal ZnO nanoring, showing uniform and perfect geometrical shape. The ring diameter is 1 to 4μm, the thickness of the ring is 10 to 30nm, and the width of the ring shell is 0.2 to 1μm ^[34]	18
Fig. 2.20 a) Structure model of ZnO and the corresponding crystal planes, showing	

the $\pm (0001)$ polar surfaces. b) to d) proposed growth process and corresponding experimental results showing the initiation and formation of the single-crystal nanoring via self-coiling of a polar nanobelt. The nanoring is initiated by folding a nanobelt into a loop with overlapped ends driven by long-range electrostatic interactions among the polar charges. Short-range chemical bonding stabilizes the coiled ring structure, and the spontaneous self-coiling of the nanobelt is driven by minimizing the energy contributed by polar charges, surface area, and elastic deformation ^[34]18

Fig. 2.21 Octa-twin composed of eight pyramidal inversion-twin crystals ^[51]19

Chapter 3

Fig. 3.1 A schematic illustration of vapor phase deposition system.....23

Chapter 4

Fig. 4.1 A illustration for the region of rich ZnO synthesized.....30

Fig. 4.2 Micrographs of ZnO tetrapods grown on AAM substrate by vapor-phase-deposition at 950°C for 10 min in air atmosphere. **a)** Aggregated ZnO tetrapods. **b)** A tilted view image of a freestanding single-crystalline ZnO tetrapod. **c)** Face-on view image of the aggregated ZnO tetrapods. **d)** High magnification image of the aggregated ZnO tetrapods. Inset in Fig. 4.2d presented hexagonal shape for the end-point of tetrapod. **e)** A bright-field TEM image of the single ZnO tetrapods. **f)** A [0001] zone-axis selected-area electron diffraction (SAED) pattern of Fig. 4.2e.....31

Fig. 4.3 Micrographs of T-ZnO nanorods grown on silicon substrate by vapor-phase-deposition at 950°C for 10min in air atmosphere. **a)** Low magnification, top view image of the sample. **b)** Tilted view image of the sample. **c)** Face-on view image of the single ZnO tetrapod. **d)** High magnification, bottom view image of the single ZnO tetrapod. **e)** A bright-field TEM micrograph of the single ZnO tetrapod. **f)** A $[01\bar{1}1]$ zone-axis selected-area electron diffraction (SAED) pattern of Fig. 4.3e...32

Fig. 4.4 Micrographs of ZnO tetrapods grown on AAM substrate by vapor-phase-deposition at 950°C for 10min in H₂O atmosphere. **a)** Low magnification, tilted view image of sample. **b)** Face-on view image of aggregated ZnO tetrapods. **c)** The aggregated ZnO tetrapods. **d)** High

magnification, face-on view of ZnO tetrapods. **e)** A bright-field TEM image of single T-ZnO nanorod. **f)** A $[\bar{1}2\bar{1}6]$ zone-axis diffraction pattern of Fig. 4.4e.....33

Fig. 4.5 ZnO nanostructures grown on silicon substrate by vapor-phase-deposition at 950°C for 10min in H₂O atmosphere. **a)** Low magnification, face-on view image of aggregated ZnO tetrapods. **b)** High magnification, armor-unit-shape ZnO tetrapods. **c)** A bright-field TEM image of single ZnO tetrapods. **d)** A $[0001]$ zone-axis selected-area electron diffraction pattern of Fig. 4.5c.....34

Fig. 4.6 Micrographs of T-ZnO nanorods grown on silicon substrate by vapor-phase-deposition at 950°C for 10min in H₂O₂ atmosphere. **a)** Low magnification, aggregated ZnO tetrapods. **b)** Coarser trumpet-shape ZnO tetrapods. **c)** Trumpet-shape ZnO tetrapod. **d)** Finer trumpet-shape ZnO tetrapods. **e)** A bright-field TEM image of single trumpet-shape ZnO nanorod. **f)** A $[\bar{1}2\bar{1}6]$ zone-axis selected-area electron diffraction (SAED) pattern of Fig. 4.6e.....35

Fig. 4.7 Micrographs of ZnO tetrapods grown on silicon substrate by vapor-phase-deposition at 950°C for 10min in H₂O₂ atmosphere. **a)** Low magnification, top view image of the tetrapods aggregation. **b)** A face-on view image of the bat-shape ZnO tetrapods. **c)** A bat-shape ZnO tetrapods. **d)** High magnification, title view image of the single rod of bat-shape T-ZnO. **e)** A bright-field TEM image of the bat-shape T-ZnO nanorod. **f)** A $[\bar{1}2\bar{1}6]$ zone-axis diffraction pattern of Fig. 4.7e.....36

Fig. 4.8 Micrographs of ZnO tetrapods grown on silicon substrate by vapor-phase-deposition at 950°C for 10min in H₂O₂ atmosphere. **a)** Top view image of large yield tetrapods on the substrate. **b)** Bamboo-shape ZnO tetrapods. **c)** Bottle-shape ZnO tetrapods. **d)** Face-on view image of the ZnO tetrapods with trumpet-shape arms.....37

Fig. 4.9 SEM micrographs of multi-rods ZnO crystals. **a)** Bat-shape ZnO multi-rods. **b)** Needle-shape ZnO multi-rods. **c)** Low magnification, face-on view image of multi-rods ZnO crystals **d)** Freestanding anemone-shape ZnO crystal.....38

Fig. 4.10 A schematic chart of the oxygen concentration v.s. the ratio of basal plane

growth to c-axis growth.....38

Fig. 4.11 SEM micrographs correspond to CL spectra for ZnO tetrapods synthesized in air atmosphere. The ZnO tetrapods dispersed on the Cu net for TEM recorded. **a)** The arrow in Fig. 4.11a points to CL detection for the individual ZnO tetrapods crystal. **b)** CL spectrum of the individual ZnO tetrapods in Fig.4.11a.....39

Fig. 4.12 SEM micrographs of the ZnO tetrapods with similar diameter in shape by synthesized in H₂O atmosphere correspond to CL spectra. **a)** Face-on view image of the freestanding ZnO tetrapods. **b)** CL spectrum of the single ZnO tetrapods in Fig. 4.12a. **c)** Face-on view image of the single ZnO tetrapods. **d)** The arrow in Fig. 4.12c points to CL detection for the individual ZnO tetrapods. **e)** Face-on view image of the aggregately ZnO tetrapods. **f)** The arrow in Fig. 4.12e points to CL detection for the individual ZnO tetrapods.....40

Fig. 4.13 SEM micrographs and corresponding to CL spectra of ZnO tetrapods synthesized in H₂O₂ atmosphere. **a)** Face-on view image of the freestanding ZnO tetrapods. **b)** The arrow in Fig. 4.13a indicates the point to CL detection of the freestanding ZnO tetrapods. **c)** Top view image of the single ZnO tetrapods. **d)** The arrow in Fig. 4.13c indicates the point to CL detection of the individual ZnO tetrapods. **e)** Face-on view image of the aggregately ZnO tetrapods. **f)** The arrow in Fig. 4.13e points to CL detection for the individual ZnO tetrapods.....41

Fig. 4.14 SEM micrographs and corresponding to CL spectra of ZnO tetrapods synthesized in H₂O₂ atmosphere. **a)** Face-on view image of the freestanding ZnO tetrapods. **b)** The arrow in Fig. 4.14a points to CL detection for the individual ZnO tetrapods. **c)** Aggregated bell-shape ZnO crystals. **d)** The arrow in Fig. 4.14c points to CL detection for the individual ZnO crystal. **e)** Freestanding diamond-shape ZnO crystal. **f)** The arrow in Fig. 4.14e points to CL detection of the individual ZnO crystal.....42

Figure 4.15 ZnO tetrapods synthesized in three ambiances exhibited different PL

spectra.43

Fig.4.16 A schematic illustration of the pyramid growth of ZnO tetrapod. **a)** A schematic illustration of ZnO cluster. **b)** A schematic illustration of ZnO tetrapod growth model.....44

Fig. 4.17 SEM images of ZnO tetrapods nucleus. **a)** A face-view image of ZnO cluster. **b)** High magnification, a face-view image of ZnO tetrapod nucleus starting to grow. **c)** A high magnification image of smaller “armor unit” shape T-ZnO. **d)** A face-on view of awl-shape ZnO tetrapod.....44

Fig. 4.18 TEM micrographs of single T-ZnO nanorod. **a)** A low magnification TEM image of the single T-ZnO nanorod. **b)** An enlarged TEM image of the single T-ZnO nanorod in Fig.4.18a. **c)** A HR-TEM micrograph of the rim side of single T-ZnO nanorod. Inset in Fig. 4.18c is a $[\bar{1}2\bar{1}6]$ zone-axis diffraction pattern of its. **d)** A high magnification HR-TEM micrograph, the lattice match image of the rim side of single T-ZnO nanorod.....45

Fig. 4.19 SEM micrographs of ZnO rods as the helical growth mechanism. **a)** Face-on view of the surface helical morphology of end-point of the individual ZnO rod. **b)** Top-view image of the ZnO rods as the helical growth. **c)** Single rod of tetrapods presented the helical growth process; inset in Figure4.19c is a condensed image of a freestanding ZnO tetrapods. **d)** Rods synthesized by helical like growth. **e)** Rods grown follow helical orientation toward one direction. **f)** End-point of the tetrapods with flow-like presented symmetrical growth.....46

Chapter 1 Introduction

1.1 A brief review

Over the last decade, progress in semiconductor research has led to the development of new materials that promise to extend the availability of versatile and inherently inexpensive light sources from the currently accessible near infrared and red regions of the spectrum into the green-blue and near ultraviolet. White light and ultra-broad band visible emission from miniature sources open up a huge range of optoelectronic applications. One-dimensional (1D) nanometer-sized semiconductor materials, such as nanowires and nanorods, have attracted considerable attention due to their great potential for fundamental studies of the roles of dimensionality and size in their physical properties as well as for their applications in optoelectronic nanodevices^[1, 5, 32, 35]. They require not only structural integrity but also high surface area. Many researches have concentrated on zinc oxide (ZnO) in thin films and particles. The growth of aligned 1D zinc oxide--a direct wide band gap ($E_g = 3.37$ eV) semiconductor with a larger excitation binding energy (60 meV) than GaN (28 meV)^[45]--nanostructure has huge promising applications for field emission, optoelectronics, and sensor arrays^[28], *etc.*

1.2 Motivation

The emitted properties of the ZnO depend closely on the microstructure of the materials, including crystal size, orientation, morphology, aspect ratio, and even crystalline density^[47]. Much effort in

literatures discussed the emitted properties of ZnO^[3, 5, 7, 9, 12, 14-16, 21, 23, 26-28, 46-48]. In nature, developing synthetic approaches to recognize ZnO emitted remains a significant challenge. Our strategy to design single-crystal rods is based entirely on self-assembly mechanism, *in-situ* and bottom-up, approach to achieve oriented geometry. As discussed above, we studied the demonstration related to its emission and geometry of ZnO nanorods and tried to discuss their correlativity.

The aims of this thesis, therefore, are as follows:

1. To grow single crystal ZnO nanorods by vapor phase deposition
2. To carry out an experimental research on the manifestation of luminescence properties and its morphologies

1.3 Organization of the thesis

The thesis consists five chapters, including the present introduction. Literature review, the methods of ZnO synthesis, and the luminescent properties of ZnO nanostructures are given in chapter 2. Chapter 3 presents our experimental details, including of sample preparation and property of characterization. The synthesis of ZnO nanostructures by vapor deposition and their structural and emitted characteristics were discussed in Chapter 4. Finally, Chapter 5 concludes our investigations on the emitted correlativity to ZnO nanostructures.

Chapter 2 Literatural Review

2.1 A Brief introduction of ZnO

ZnO—a direct wide band gap ($E_g = 3.37$ eV) II-VI semiconductor with a larger excition binding energy (60 meV) than ZnSe (22 meV) and GaN (28 meV) ^[1, 2] —is suitable for transparent to visible light, and can be made highly conductivity by doping. ZnO is one of the most important functional oxide and has high potential applications for nano-materials, exhibiting near-UV emission, transparent EMI shielding, supercapacitors, photo-catalyst ^[3], multifunctional nanocomposites ^[4], Sound insulation, photosensitization, gas sensors ^[5], resonator ^[6], piezoelectric, laser diodes (LDs) ^[7], light-emitting diodes (LEDs), transducers ^[8], surface acoustic wave devices ^[9], and hydrogen storage ^[10], *etc.*

During the last decades, many efforts have been invested in controlling the sizes and shapes of inorganic nanocrystals, because these parameters are critical in determining their electrical and optical properties ^[11, 12]. One-dimensional (1D) nanomaterials have attracted great interests due to their importance in basic scientific research and potential technological applications ^[13]. Other than carbon nanotubes, 1D nanostructure such as nanowires and nanorods are ideal systems for investigating the dependence of electrical transport, optical and mechanical properties on size and dimensionality. Many fascinating and unique properties have already been proposed or demonstrated for this class of materials, such as higher luminescence efficiency ^[14], superior mechanical toughness ^[15], a lowered lasing threshold, enhancement of

thermoelectric figure of merit ^[16], and even heterostructures in GaN/ZnO ^[17, 18]. The trend in developing short-wave-length semiconductor laser has culminated in the realization of room-temperature green-blue diode laser structures with ZnSe, InGaN, and ZnO as the active layers. Undoubtedly, ZnO nanostructures—an oxide accessibly synthesized by vapor phase deposition in furnace— would combine with conducting polymer to form emission materials in the future.

2.2 Fabrication Methods of Oriented ZnO

Many researches presented the oriented array of nanorods on various substrates—sapphire ^[7, 19-24] and silicon wafer ^[25-30]. These techniques have already been demonstrated by the fabrication of large, three-dimensional arrays of ZnO, in which a microchip equipped with nano-scale light sources and sensors.

Up to now, physical deposition ^[1, 3, 4, 6, 7, 12, 19-27, 29, 32-34, 36-38], aqueous solution ^[31, 39-42], electrochemical deposition in porous alumina-membrane template ^[35, 43, 44], and pulsed laser deposition ^[45], have been successfully produced the oriented anisotropic nanorods of ZnO. The horizontal quartz-tube furnace method, which is popular for the synthesis of ZnO nanostructures, is shown in Fig. 2.1. In 2001, Michael H. Huang employed this method to synthesize ZnO nanowire nanolasers ^[7], and their results are shown in Fig. 2.2. In 2003, H. Yan et al. adopted used the Zn powder as Zn vapor source and the mixture of 0.5-5% O₂/Ar gas flow at 800-900°C for 10-30 min to synthesize armor-unit-shaped ZnO tetrapods, and employed the mixture of 5-10% O₂/Ar gas flow to synthesize trumpet-shaped ZnO tetrapods, as shown in Figs. 2.3 and 2.4.

Further, they used a 1:1 ZnO/C mixture as vapor source to synthesize the ZnO tetrapods with trumpet-like arms ^[11], as shown in Figs. 2.5 and 2.6. V. A. L. Roy synthesized ZnO tetrapods by employing different gas flow— air, dry argon (Ar) flow, and wet Ar flow— and used Zn powder as source at 950°C in tube furnace, as shown in Fig. 2.7. Nanostructures had smaller average sizes in humid argon flow than tetrapod nanostructures obtained in air ^[32]. In February 2004, V. A. L. Roy again presented ZnO tetrapods of new morphology by doped Mn in ZnO vapor source shown in Fig. 2.8, it not only reduced the size of ZnO tetrapod but also increased the magnetization of ZnO by Mn doping ^[46]. In April 2004, Djurisic reported the ZnO tetrapod synthesized by using the Zn, ZnO:C, and ZnO:C:GeO₂ respectively ^[47], and their results are shown in Fig. 2.9.

2.3 Luminescent Properties of Oriented ZnO

As shown in Fig. 2.10, V. A. L. Roy demonstrated that different conditions of experiments imply different emission properties of ZnO tetrapods. Nanostructures fabricated in wet Ar flow exhibited higher UV than green emission and had smaller average sizes than tetrapods prepared in air ^[32]. V. A. L. Roy also found that Mn doping does not change the positions of emission peak. Mn doping is expected to reduce the intensity of UV emission and increase the intensity of green emission ^[46] see in Fig. 2.11. Djurisic and Leung found that all their samples possess UV and broad green emission peaks. The pure ZnO samples had very similar photoluminescence (PL) spectra, while the samples prepared from a ZnO:C: GeO₂ mixture show very strong green PL and intensity of green peak increases with the increase of GeO₂ concentration in the

source material ^[47], as shown in Fig. 2.12.

Nevertheless, B. D. Yao synthesized ZnO nanostructures using pure ZnO powder mixed with graphite (molar ratio 1:1) without any catalyst. The nanowires and nanorods exhibited completely different luminescence spectra, as shown in Figs. 2.13 and 2.14. The nanowires with 200 nm in diameter show strong UV emission and negligible green emission ^[26]. Ng presented completely different results, shown in Figs. 2.15 and 2.16. They synthesized ZnO nanostructures using a 1:1 mixture (by weight) of ZnO and graphite powder as vapor source and m-sapphire as substrate on which a pre-sputtered Au thin film (20 Å) served as the catalyst. The ZnO nanowire with 222 nm in diameter exhibited UV emission and green emission, which corresponds to half intensity of UV emission ^[48]. According to their researches, we suggested that the ZnO phosphor emission should not be affected by the morphologies of nanostructures. The relationship between emission properties and morphologies of ZnO nanostructures are discussed in Ch4.

2.4 Crystal Structure and Growth Mechanism of Oriented ZnO

ZnO has a hexagonal wurtzite structure with lattice parameters $a = 0.3296$ and $c = 5.207$ nm. The structure of ZnO can be simply described as a number of alternating planes composed of tetrahedrally coordinated O^{2-} and Zn^{2+} ions, stacked alternately along the \vec{c} -axis, as shown in Fig. 2.17.

The tetrahedral coordination of ZnO results in non-central symmetric

structure and consequently piezoelectricity and pyro-electricity; polar surfaces are another important characteristic of ZnO. The basal plane is the most common polar surface of ZnO ^[50].

ZnO structures have three types of fast growth directions: $\langle 2\bar{1}\bar{1}0 \rangle$ ($\pm [2\bar{1}\bar{1}0]$, $\pm [\bar{1}2\bar{1}0]$, $\pm [\bar{1}\bar{1}20]$); $\langle 01\bar{1}0 \rangle$ ($\pm [01\bar{1}0]$, $\pm [10\bar{1}0]$, $\pm [\bar{1}100]$); and $\pm [0001]$. Aggregation on the polar surfaces due to atomic terminations, ZnO structures exhibit a wide range of novel structures that can be grown by tuning the grown rates along these directions; one of the most profound factors determining the morphology is the relative surface activities of various growth facets under the given conditions. Perceivably, a crystal has different kinetic parameters for different crystal planes, which are emphasized under harnessed growth conditions. Therefore, after an initial period of incubation and nucleation, nucleus will commonly develop into a 3-D object with well-defined, low index crystallographic faces. Figures 2.18(a)-(c) show a few typical growth morphologies of 1-D nanostructures for ZnO. These nanostructures tend to maximize the areas of the $\{2\bar{1}\bar{1}0\}$ and $\{01\bar{1}0\}$ facets because of the low surface energy. The morphology shown in Fig. 2.18 (d) is dominated by the polar surfaces, which can be grown by introducing planar defects parallel to the polar subfaces; planar defects and twins are observed occasionally parallel to the (0001) plane ^[50].

Indeed, Z. L. Wang's group proposed not only the vapor-solid (VS) growth mechanism but also spiral growth mechanism for ZnO nanostructures. As shown in Figs. 2.19 and 2.20, a freestanding single-crystal nanoring of ZnO was grown by a solid-vapor process, and the coiling of the nanobelt at a small helical angle of about 0.3° developed

the nanoring ^[34]. At the same time, Yue Zhang and co-workers proposed a pyramid-like growth mechanism, octa-twins nuclei consist of eight tetrahedral crystals each consisting of three $\{1\bar{1}2\}$ pyramidal faces and one $\{0001\}$ basal face as shown in Fig. 2.21. The eight tetrahedral crystals connected together by making the pyramidal faces contact one another to form an octahedral crystal ^[51].



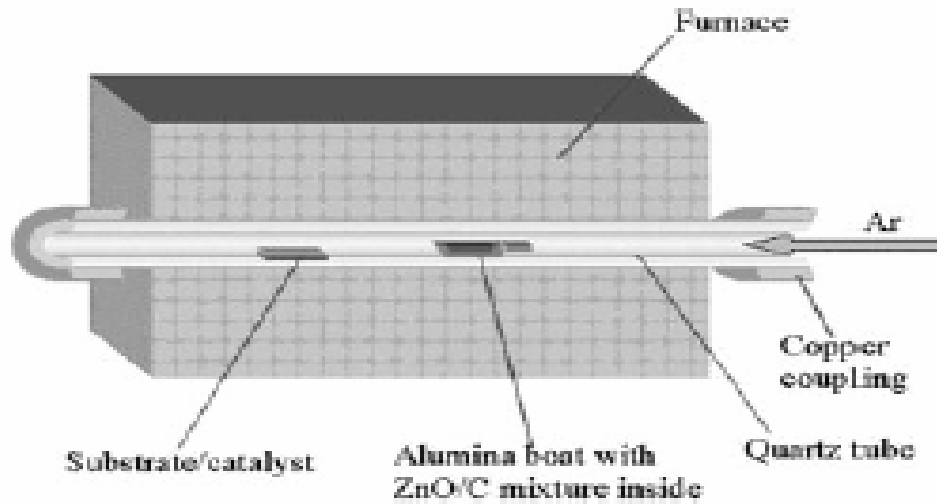


Figure 2.1 Schematic illustration of the chemical vapor transport and condensation experimental set-up for ZnO nanowire growth ^[1].

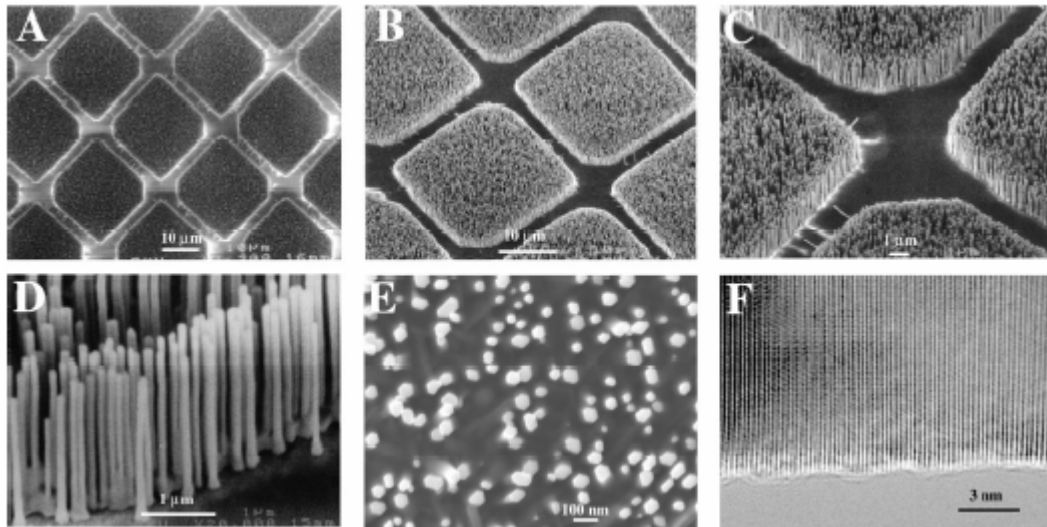


Figure. 2.2 (A through E) SEM images of ZnO nanowire arrays grown on sapphire substrates. A top view of the well-faceted hexagonal nanowire tips is shown in (E). (F) High-resolution TEM image of an individual ZnO nanowire showing its <0001> growth direction ^[7].

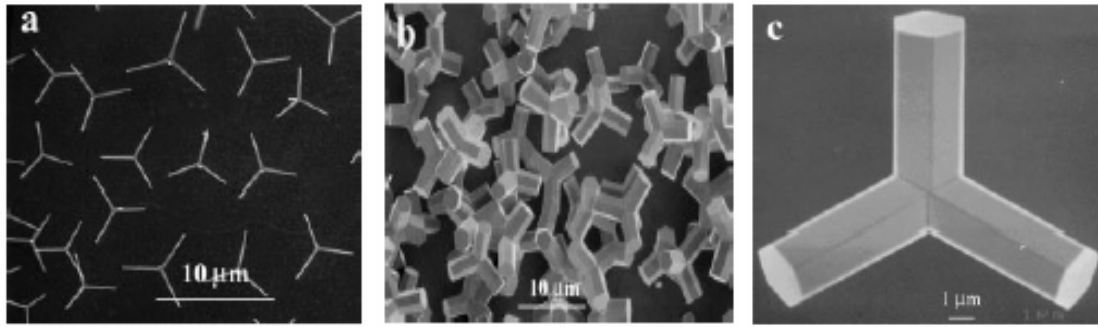


Figure 2.3 SEM images of ZnO tetrapods with different diameters. **a)** ZnO tetrapods with arms of 200 nm diameter. **b)** ZnO tetrapods with arms of 2 μm diameter. **c)** High-magnification SEM image of a single ZnO tetrapod with an arm of 2 μm diameter ^[11].

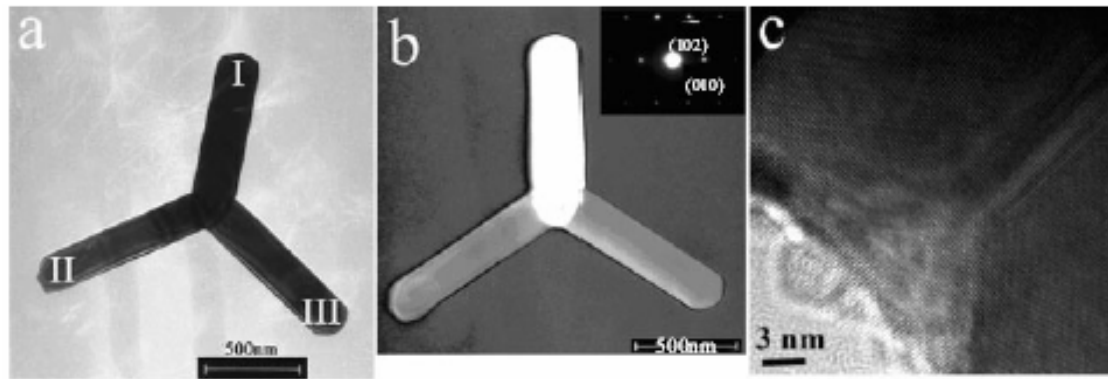


Figure 2.4 **a)** TEM image of a tripod. **b)** Dark field image of arm I recorded on the $[10\bar{2}]$ spot along the $[201]$ zone axis. The inset is the SAD pattern of arm I of the tripod. **c)** High-resolution TEM image at the joint of the tripod ^[11].

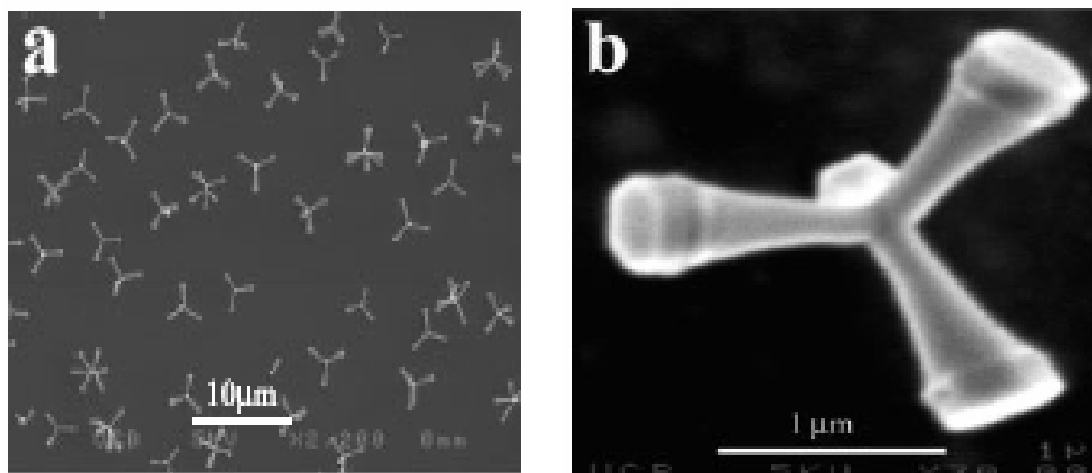


Figure 2.5 SEM images of ZnO tetrapods with trumpet-like arms at low **(a)** and **(b)** magnification ^[11].

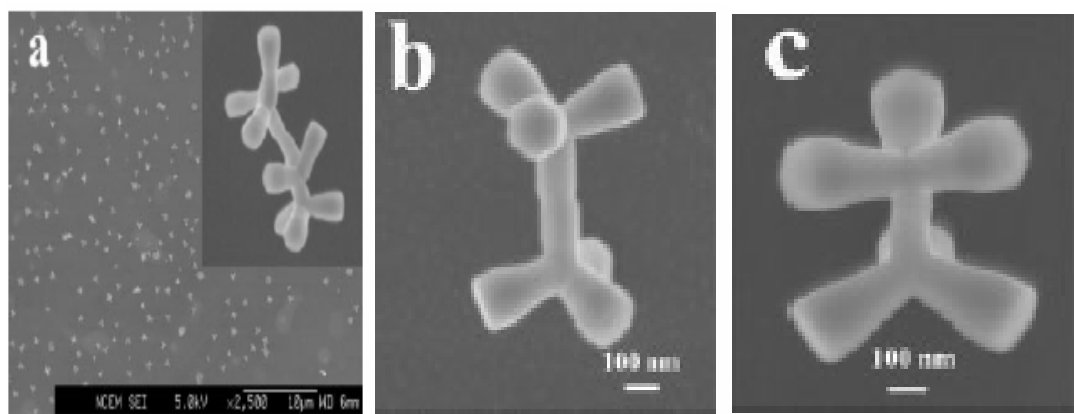


Figure 2.6 SEM images of self-assembled ZnO tetrapods. **a)** A Low-magnification SEM image of ZnO tetrapods with trumpet-shaped arms. The inset image is a tetramer formed from the ZnO tetrapods. **b)** Staggered view of the ZnO tetrapod dimer. **c)** Eclipsed view of the ZnO tetrapod dimer^[11].

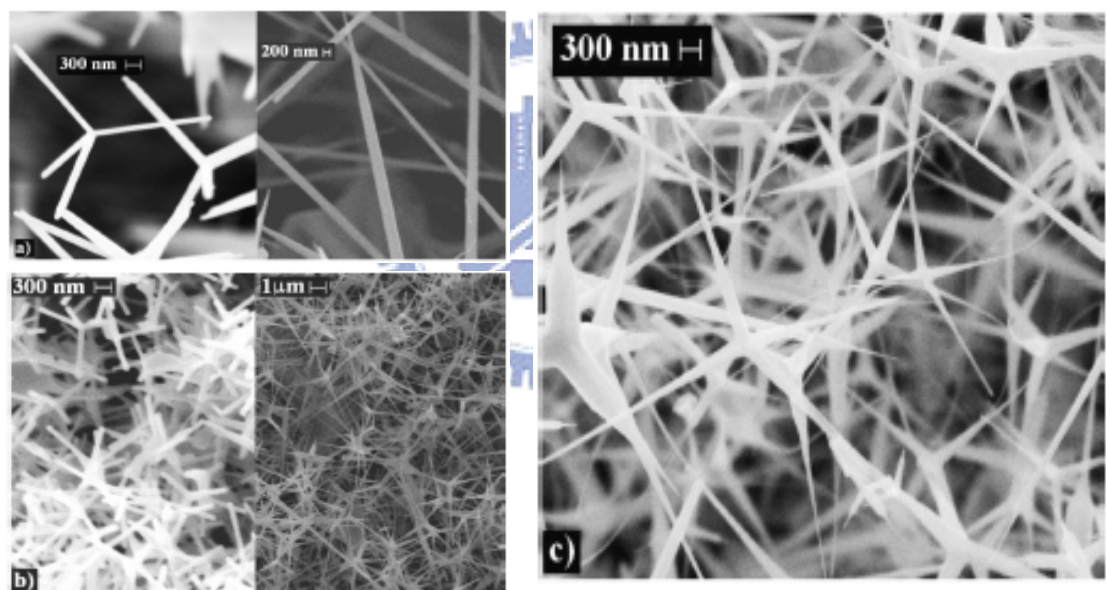


Figure 2.7 SEM images of ZnO nanostructures: **a)** tetrapods (left) and rods (right) obtained in air; **b)** small tetrapods (left) and mixture of tetrapods and wires (right) obtained in dry argon flow; and **c)** mixture of tetrapods and wires obtained in humid argon flow^[32].

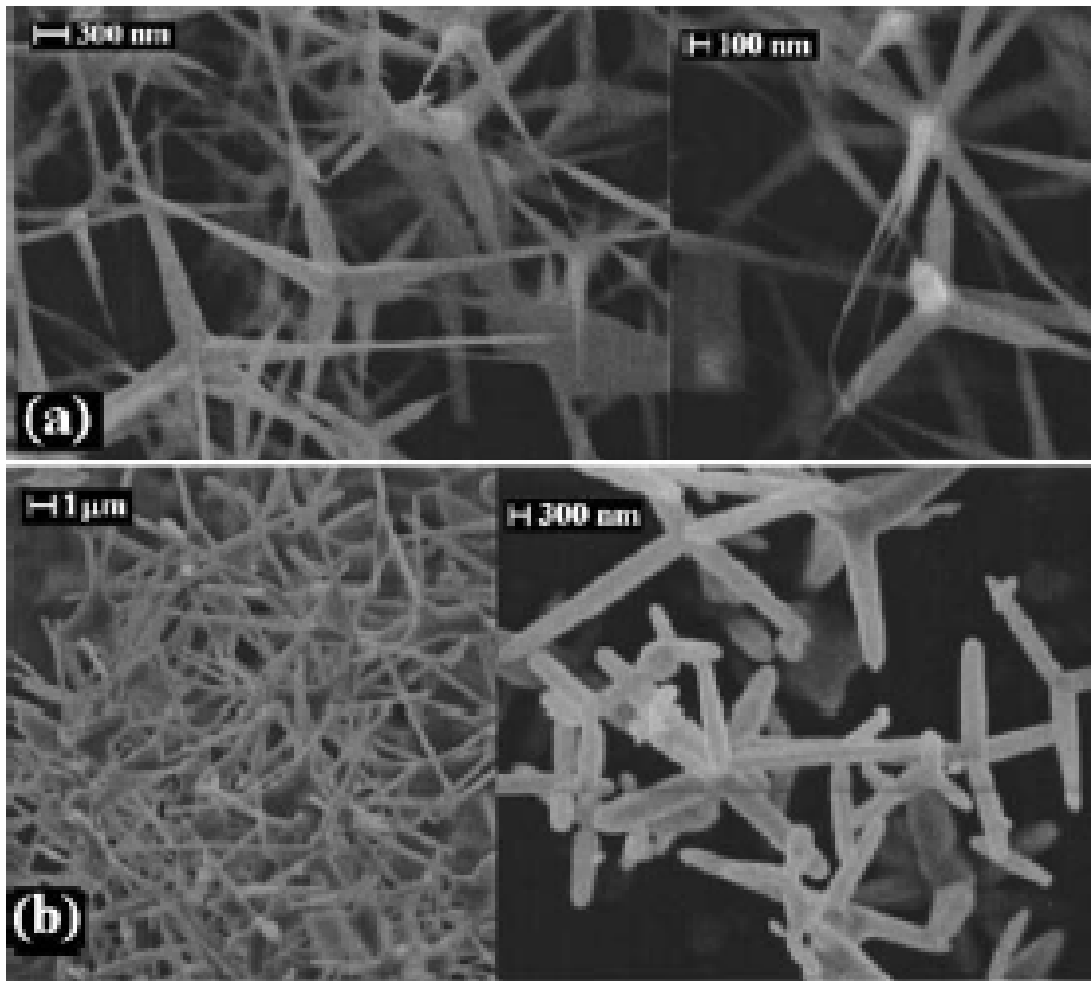


Figure 2.8 Representative SEM images of **a)** undoped ZnO, **b)** Mn diffusion doped ZnO ^[46].

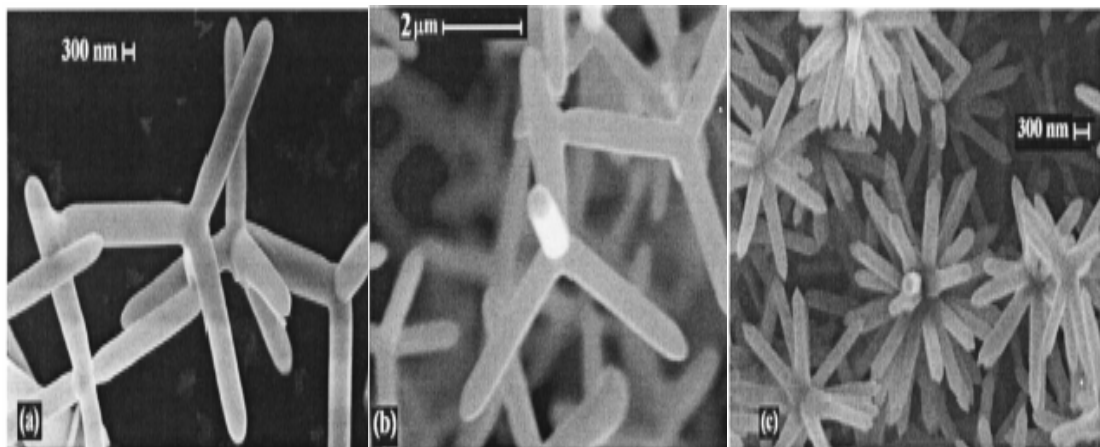


Figure 2.9 Representative SEM images of ZnO nanostructures: **a)** ZnO prepared from Zn. **b)** ZnO prepared from ZnO:C. **c)** ZnO prepared from ZnO:C:GeO₂ ^[47].

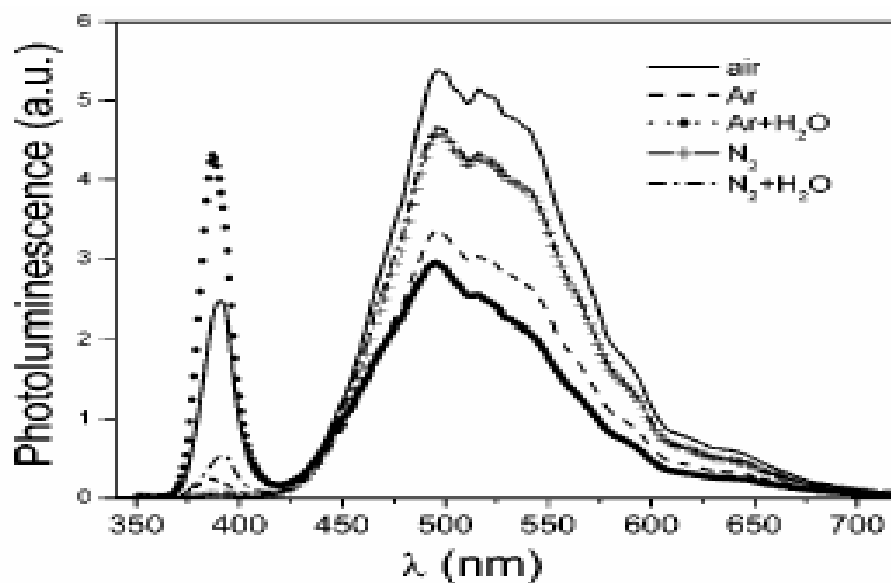


Figure 2.10 Photoluminescence of ZnO nanostructures prepared under different conditions ^[32].

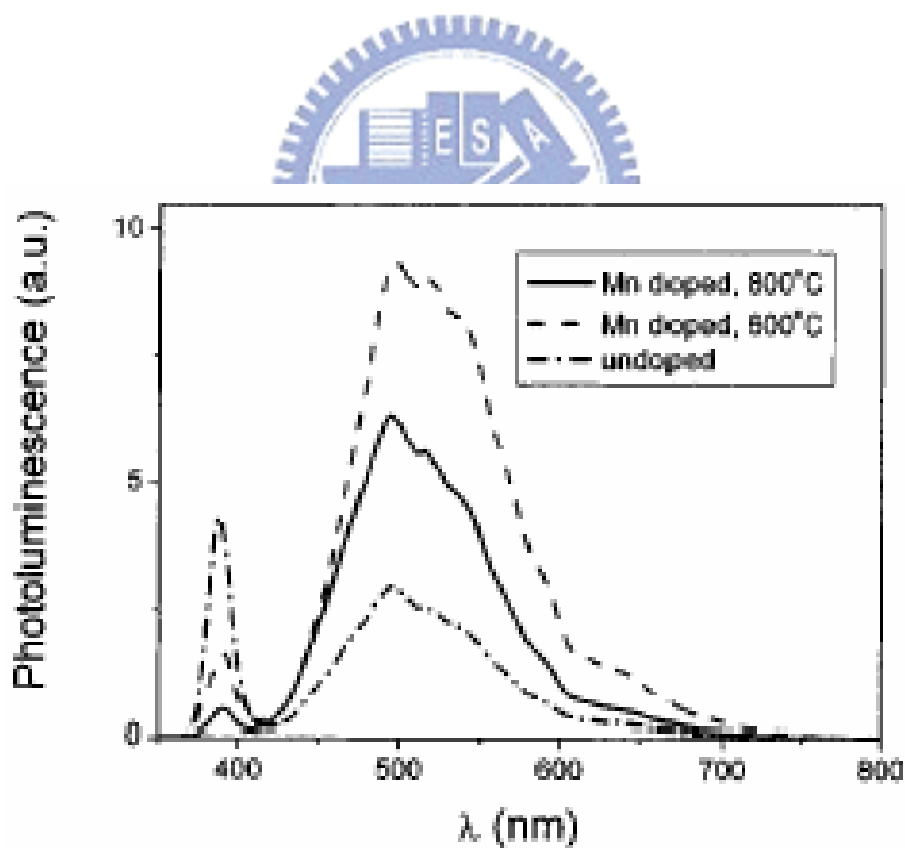


Figure 2.11 Photoluminescence of undoped and Mn doped ZnO tetrapod structures ^[46].

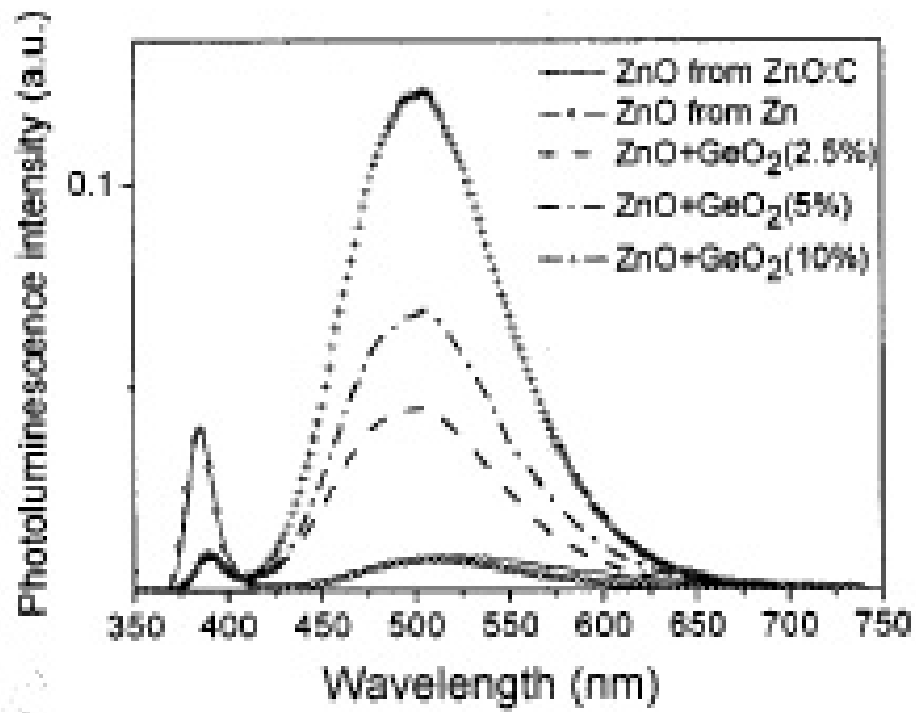
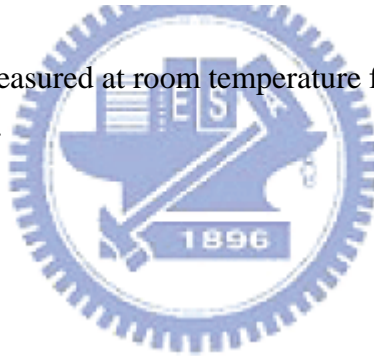


Figure 2.12 PL spectrum measured at room temperature from ZnO structures prepared from different materials ^[47].



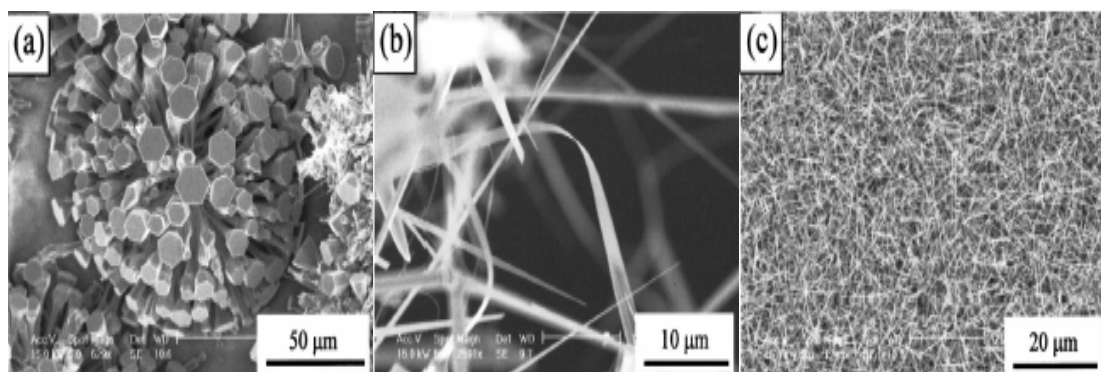


Figure 2.13 SEM images showing the three typical morphologies of the as-prepared ZnO products. **a)** needle-like rods. **b)** nanoribbons. **c)** nanowires^[26].

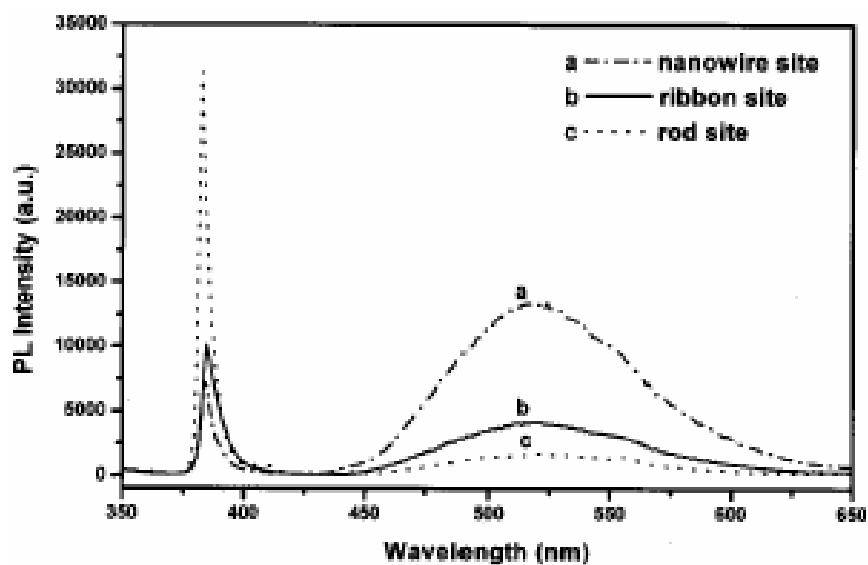


Figure 2.14 PL spectra recorded at room temperature. Spectra a, b, and c were recorded from the low temperature site nanowires, the medium temperature site nanoribbons, and the high temperature site needle-like rods, respectively^[26].

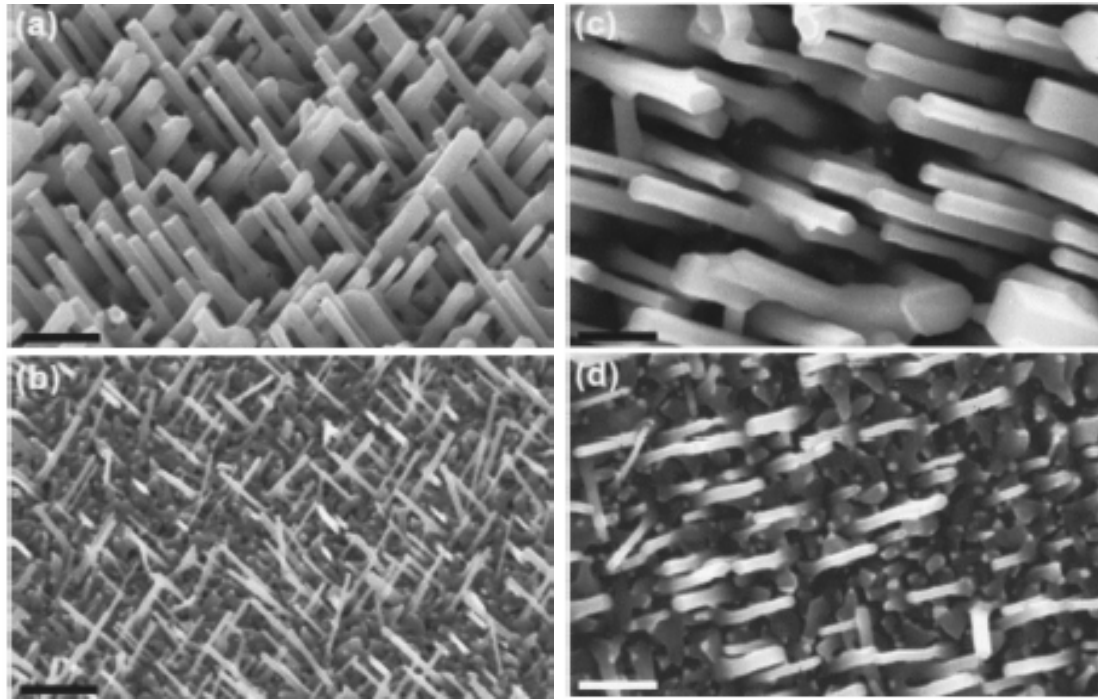


Figure 2.15 FE-SEM images of ZnO nanowire arrays on m-sapphire. **a)** and **b)** perspective view (45°) of the nanowires with growth duration 30 and 10 min, respectively. Scale bar: 1 μm . **c)** and **d)** corresponding top views. Scale bar: 500 nm ^[48].

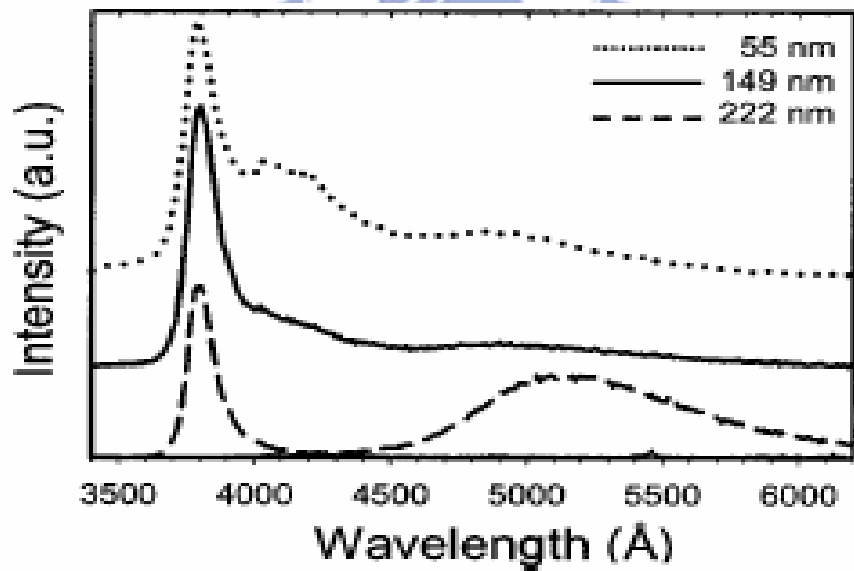


Figure 2.16 Photoluminescence spectra of ZnO nanowires at room temperature using 325 nm line of a He-Cd laser as the excitation source ^[48].

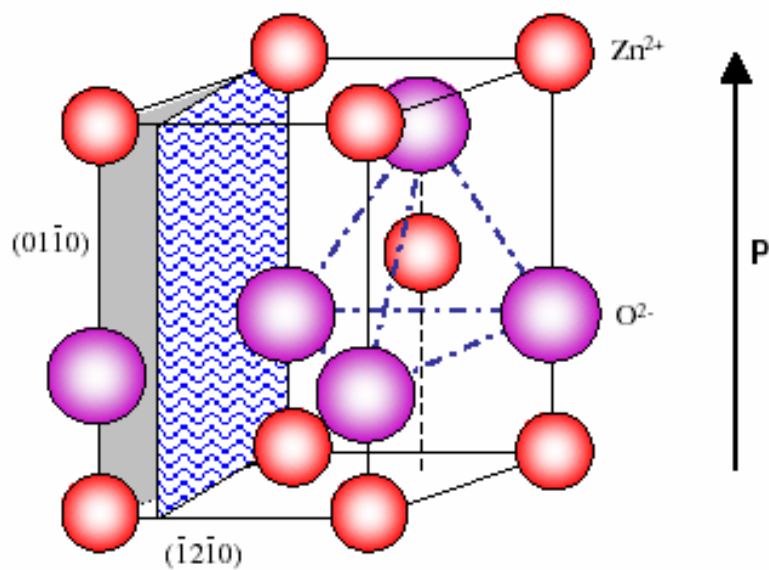


Figure 2.17 The wurtzite structure model of ZnO. The tetrahedral coordination of Zn-O is shown ^[50].

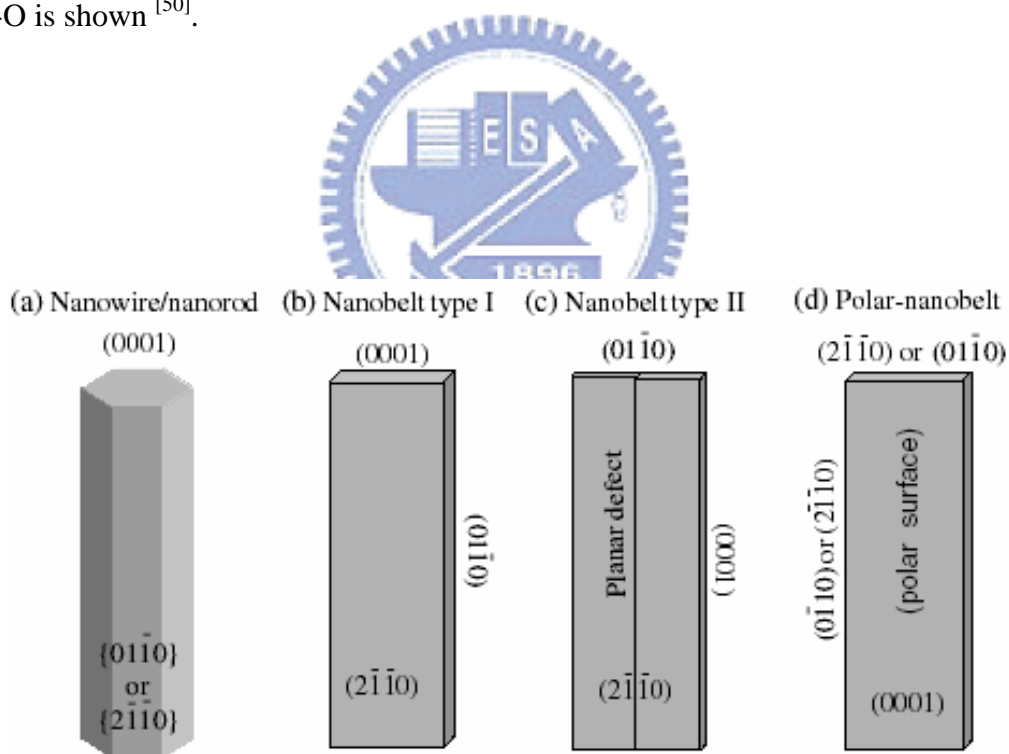


Figure 2.18 Typical growth morphologies of one-dimensional ZnO nanostructures and the corresponding facets ^[50].

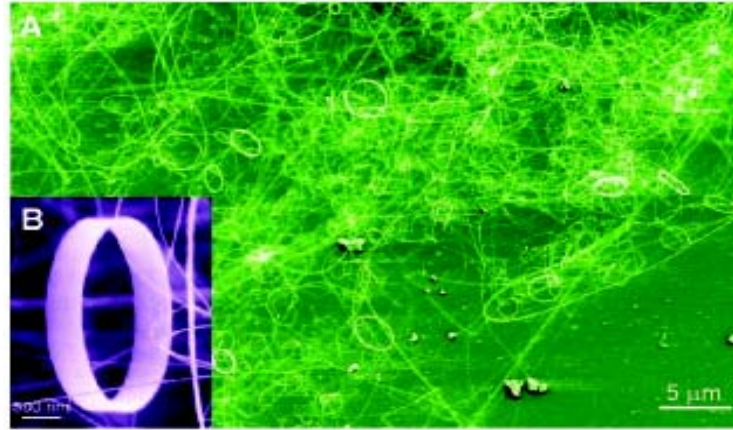


Figure 2.19 **a)** Low-magnification SEM image of the as-synthesized ZnO nanorings. **b)** High-magnification SEM image of a freestanding single-crystal ZnO nanoring, showing uniform and perfect geometrical shape. The ring diameter is 1 to 4 μm , the thickness of the ring is 10 to 30 nm, and the width of the ring shell is 0.2 to 1 μm ^[34].

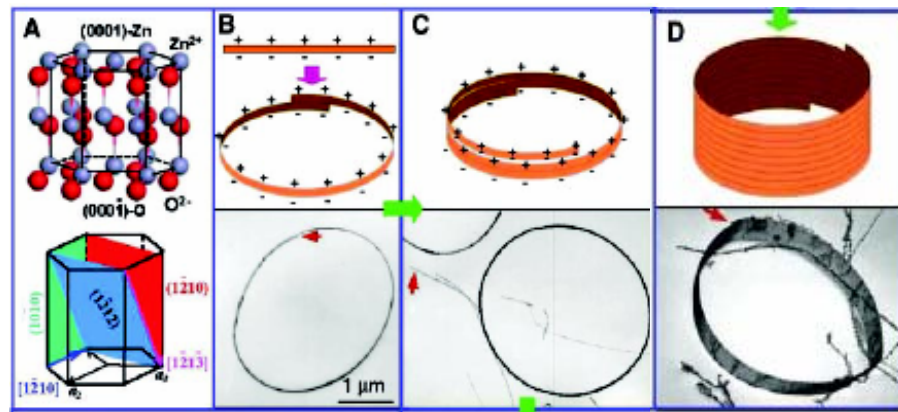


Figure 2.20 **a)** Structure model of ZnO and the corresponding crystal planes, showing the $\pm(0001)$ polar surfaces. **b) to d)** proposed growth process and corresponding experimental results showing the initiation and formation of the single-crystal nanoring via self-coiling of a polar nanobelt. The nanoring is initiated by folding a nanobelt into a loop with overlapped ends driven by long-range electrostatic interactions among the polar charges. Short-range chemical bonding stabilizes the coiled ring structure, and the spontaneous self-coiling of the nanobelt is driven by minimizing the energy contributed by polar charges, surface area, and elastic deformation ^[34].

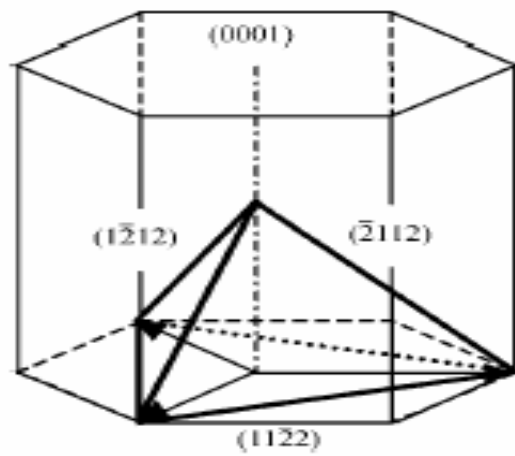


Figure 2.21 Octa-twin composed of eight pyramidal inversion-twin crystals ^[51].



Chapter 3 Experimental Process

The ZnO tetrapods synthesized in this work is based on the vapor deposition of Zn-O vapor under the harnessing conditions without the presence of fresh gas flow. To obtain the ZnO tetrapods, we demonstrated a method different from previous studies to grow ZnO tetrapods in open furnace system. The experiment employed vertical thermal vapor deposition with a one-end sealed quartz tube covered with a steel cup in box furnace and controlled the ambiance of furnace —the ratio of H₂O vapor, H₂O₂ vapor, and air atmospheres— in the quasi-closed system to produce the various oriented ZnO tetrapods.

3.1 Experimental Apparatus

A one-end-sealed quartz tube with 92 mm in length and 15 mm in inner diameter (volume = 16.26 cm³), a cup with 25 mm in external diameter, 16 mm in internal diameter, and 5 mm in thickness manufactured from 310 stainless steel, and a C-ring with 16 mm in external diameter to fix the sample, silicon with 15 mm in diameter and alumina membrane (AAM, commercial template) template were constituted the apparatus of this experiment, as shown in Fig. 3.1. A box furnace was adopted as thermal source. Zn pellets (99.9999%) with 954 mg in weight (1.39×10^{-2} mole) were used as Zn vapor source.

3.2 Sample Preparation

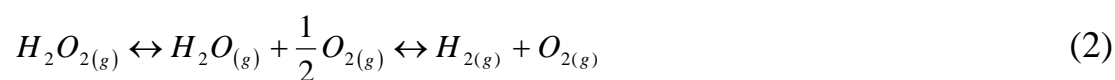
Experimental Procedures

1. Silicon wafer was cleaned in a sonicating bath of acetone for 30 min.
Zn pellets (954 mg) were used as Zn source; an equal amount, 954 mg in weigh, of Zn pellets placed at the sealed end of a one-end-sealed quartz tube.
2. The substrate, silicon wafer or AAM, fixed in the C-ring was placed on the steel cup.
3. The tube was loaded into furnace when the furnace was heated to 950°C. The reaction was carried out at 950°C for 10min.
4. After the reaction, the tube was took out from furnace and cooled in air naturally.

The experiments were carried out at three different ambiances described as follows to obtain various morphology of ZnO tetrapod :

1. The tube with the air at 1 atm.
2. To fill with the deionised water, 16.26c.c, into the tube at 1atm.
3. To fill with the hydrogen peroxide liquid, 16.26c.c, into the tube at 1atm.

The decomposition equation of the deionised water and hydrogen peroxide can be expressed as:



The equilibrium partial oxygen pressure could be calculated from

$$\Delta G_f^o = RT \ln K, \quad \log K = \log P_{H_2} + \frac{1}{2} \log P_{O_2} - \log P_{H_2O} \quad \text{and}$$

$$\log K = \log P_{H_2} + \log P_{O_2} - \log P_{H_2O_2}.$$

	air	H ₂ O	H ₂ O ₂
$P_{O_2} (atm)$	0.21	4.6837×10^{-6}	0.8386atm

3.3 Characterization of the Morphologies, Structures, and Emission Properties

Scanning Electron Microscopy (SEM)

The SEM characterization was carried out by using a JEOL JSM-6500F. Samples were coated with platinum (Pt) using a JEOL JFC-1300.

Transmission Electron Microscopy (TEM)

The TEM characterization was carried out in a transmission electron microscope (PHILIPS, TECNAI 20) operating at 200kV.

Cathodoluminescence detection system (CL)

The room-temperature CL (JEOL, JSM-6330 TF) detection was performed at an acceleration voltage of 10 kV.

Photoluminescence detection system (PL)

The PL properties were performed for powder samples pumped optically by a Micro-PL, which provided short pulses at a wavelength of 325 nm He-Cd laser.

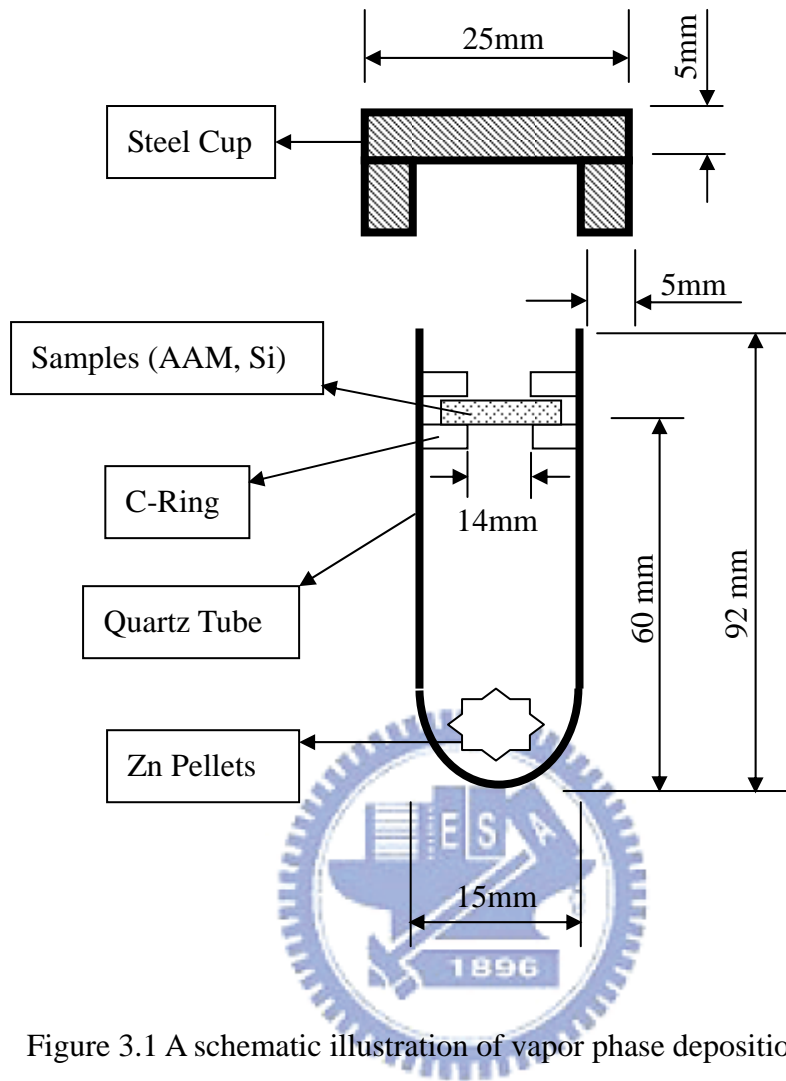


Figure 3.1 A schematic illustration of vapor phase deposition system.